Cellular and Molecular Bioengineering (© 2022)
https://doi.org/10.1007/s12195-022-00737-9

S.I. : 2022 CMBE Young Innovators

Plant Tissue Parenchyma and Vascular Bundles Selectively Regulate Stem Cell Mechanosensing and Differentiation

Kathryn Driscoll,[1] Maya S. Butani,[1] Kirstene A. Gultian,[1] Abigail McSweeny,[1] Jay M. Patel,[2,3] and Sebastián L. Vega [1]

[1]Department of Biomedical Engineering, Rowan University, Glassboro, NJ 08028, USA; [2]Department of Veterans Affairs, Atlanta VA Medical Center, Decatur, GA 30033, USA; and [3]Department of Orthopaedics, Emory University School of Medicine, Atlanta, GA 30329, USA

(*Received 18 February 2022; accepted 9 August 2022*)

Associate Editor Michael R. King oversaw the review of this article.

Abstract

Introduction—Plant tissues are plentiful, diverse, and due to convergent evolution are structurally similar to many animal tissues. Decellularized plant tissues feature microtopographies that resemble cancellous bone (porous parenchyma) and skeletal muscle (fibrous vascular bundles). However, the use of plant tissues as an inexpensive and abundant biomaterial for controlling stem cell behavior has not been widely explored.

Methods—Celery plant tissues were cut cross-sectionally (porous parenchyma) or longitudinally (fibrous vascular bundles) and decellularized. Human mesenchymal stem cells (MSCs) were then cultured atop plant tissues and confocal imaging of single cells was used to evaluate the early effects of microtopography on MSC adhesion, morphology, cytoskeletal alignment, Yes-associated protein (YAP) signaling, and downstream lineage commitment to osteogenic or myogenic phenotypes.

Results—Microtopography was conserved post plant tissue decellularization and MSCs attached and proliferated on plant tissues. MSCs cultured on porous parenchyma spread isotropically along the periphery of plant tissue pores. In contrast, MSCs cultured on vascular bundles spread anisotropically and aligned in the direction of fibrous vascular bundles. Differences in microtopography also influenced MSC nuclear YAP localization and actin anisotropy, with higher values observed on fibrous tissues. When exposed to osteogenic or myogenic culture medium, MSCs on porous parenchyma had a higher percentage of cells stain positive for bone biomarker alkaline phosphatase, whereas myoblast determination protein 1 (MyoD) was significantly upregulated for MSCs on fibrous vascular bundles.

Conclusions—Together, these results show that plant tissues are an abundant biomaterial with defined microarchitecture that can reproducibly regulate MSC morphology, mechanosensing, and differentiation.

Keywords—Plant tissues, Microarchitecture, Biophysical signals, Mechanotransduction, Stem cell differentiation.

Address correspondence to Sebastián L. Vega, Department of Biomedical Engineering, Rowan University, Glassboro, NJ 08028, USA. Electronic mail: vegas@rowan.edu

Sebastián L. Vega is an Assistant Professor in the Department of Biomedical Engineering at Rowan University with a secondary appointment in the Department of Orthopaedic Surgery at Cooper Medical School of Rowan University. His lab focuses on the design of tunable biomaterials to control cell-material interactions with applications in cell manufacturing and regenerative medicine. Sebastian's research is supported by grants from the NSF, NIH, Camden Health Research Initiative, and Cooper Foundation. Prior to joining Rowan, Sebastian was a postdoctoral researcher in Bioengineering at Penn under the mentorship of Dr. Jason Burdick, where he studied the role of biophysical and biochemical cues on matrix mechanosensing and stem cell differentiation. Sebastian completed two B.S. degrees in Chemical Engineering and Biomedical Engineering at Carnegie Mellon University and received his Ph.D. in Chemical and Biochemical Engineering from Rutgers University. As a Chilean native and first-generation Ph.D. graduate, Sebastian is passionate about initiatives that promote diversity, equity, and inclusion. Sebastian is the Chair of Outreach and Community Engagement in his department and runs in-person and virtual programs that provide diverse high school students with opportunities to learn about biomedical engineering and to conduct academic research in engineering and biomedical science labs. To learn more about the lab's work, please follow @theVegaLab on Twitter.

Published online: 20 September 2022

INTRODUCTION

Annually, an estimated 20 million animals are sacrificed in biomedical research in the United States, raising questions about ethics and sustainability.[35] Due to convergent evolution, nature has designed a wide dichotomy of natural biomaterials with a variety of biochemical and microarchitectural features.[13,17] The plant kingdom offers an inexpensive and bioethical source of natural and biocompatible scaffolds that can be used to control cell-material interactions of adherent cells.[2,18] For example, Modulevsky and coworkers implanted decellularized plant material in mice and showed a typical foreign body reaction which dissipated within eight weeks, along with fibroblast migration, deposition of new collagen extracellular matrix, and blood vessel formation within the plant-based biomaterial.[27] On a microscopic level, decellularized plant tissue microarchitecture resembles the complexity of native Mammalian tissues,[6] and as such studies have reported their use as natural biomaterials for cell culture. The microarchitecture of apple hypanthium resembles cancellous bone, and these plant tissues have been shown to support adhesion and regulate the morphology of mouse NIH3T3 fibroblasts and C2C12 muscle myoblasts.[28] When C2C12 cells are cultured on highly aligned green-onion plant tissues, they align and differentiate into cohesive myotubular networks.[5] Gershlak *et al.* also showed that decellularized spinach leaves can be repopulated with functional pluripotent stem cell-derived cardiomyocytes and mesenchymal stem cells (MSCs).[12] Although decellularized plant tissues support stem cell culture,[12,29] decoupling the effects of topographical features of plant tissues on stem cell mechanosensing and differentiation has not been widely explored.

Stem cells are adherent cells that are highly responsive to physical properties of their surrounding environment.[14] Cell-material interactions regulate early changes in stem cell morphology and mechanosensing, leading to downstream lineage commitment.[31] To explore the role of morphology on MSC differentiation, McBeath and coworkers used microcontact printing to create adhesive islands of different sizes to control the area of single cell attachment.[24] They found that larger MSCs had increased levels of GTPase RhoA and Rho kinase (ROCK), a Rho effector involved in myosin-based cytoskeletal contractility.[21] Consequently, the cytoskeleton of MSCs was more aligned and contractile. If cells are confined to morphologies that enhance or reduce cytoskeletal alignment, MSCs preferentially differentiate into osteoblasts or adipocytes, respectively.[20,24] Stem cell shape is also closely related to the organization of mechanosensitive proteins including Yes-associated protein (YAP).[10] YAP is a transcriptional regulator that transmits mechanical signals to the nucleus.[10,15] YAP is ubiquitous, constantly shuttling between the cytoplasm and nucleus of small cells, and it accumulates in the nucleus of larger cells. The role of YAP on topography-guided stem cell differentiation has also been widely studied,[16] and the effects of microtopography on stem cell differentiation is also well documented.[4,8,9,19,34] For example, MSCs cultured on continuous patterns expressed increased bone biomarker (alkaline phosphatase, ALP) expression when compared to MSCs cultured on discontinuous patterns.[32]

While the effects of microtopography on early changes in stem cell morphology, mechanosensing, and ultimately, differentiation are highly understood, it remains unclear whether microtopography of plant tissues can be used to guide stem cells to distinct mechanosensitive states and phenotypes. Celery (*Apium graveolens* L.) is an inexpensive and highly available vegetable, consisting of a root that splits into leaf-topped stalks.[22,30] The stalks consist of parenchyma and collenchyma cells within highly aligned microfibrils and vascular bundles that contain xylem and phloem to facilitate nutrient and water transfer.[3,7,32] The microarchitecture of celery stalks has unique features depending on its orientation. A longitudinal cut of celery stalks exposes vascular bundles which highly resemble fibrous structures present in connective tissues including skeletal muscle.[23] In contrast, a cross-sectional cut of the stalk exposes a porous plane, with pore diameters and roundness concomitant with cancellous bone.[26]

The goal of this study is to leverage the ability to create two distinct natural biomaterials derived from the same plant tissue to evaluate cell-material interactions of mesenchymal stem cells (MSCs). Celery stalks were cut cross-sectionally (porous parenchyma) or longitudinally (fibrous vascular bundles) prior to decellularization. Human MSCs were cultured atop porous and fibrous tissues, and MSCs adhered and proliferated on collagen-coated celery tissues. After 3 days, confocal images of labeled single cells were used to assess early changes in morphology (area, roundness, aspect ratio) and mechanosensing (actin alignment/anisotropy, nuclear YAP localization) due to porous and fibrous microarchitectures. Due to the porous and fibrous plant tissue resemblance to native human cancellous bone and muscle, preferential MSC lineage commitment to osteogenic (bone) or myogenic (muscle) was also studied. MSCs were cultured on porous or fibrous celery tissues in either osteogenic (OS) or myogenic (MYO) medium and stained with alkaline phosphatase (ALP, bone) and myoblast determination protein 1 (MyoD, muscle) biomarkers after 7 days in culture.

MATERIALS AND METHODS

Celery Plant Tissue Decellularization

Celery stalks were cut cross-sectionally or longitudinally using a mandolin slicer (2 mm thickness) and then cut into cylinders using a biopsy punch (8 mm diameter). Cylindrical celery tissue samples were placed in a 5% bleach (v/v) and 3% sodium bicarbonate (w/v) solution in deionized water and warmed to 70 °C. The samples were stirred gently until cleared, as determined visually by the loss of tissue pigmentation. Unless otherwise noted, all samples were incubated in a 4% (v/v) rat tail collagen in phosphate-buffered saline (PBS) for 24 h prior to cell seeding.

Decellularized Celery Plant Tissue Characterization

Decellularization was confirmed by the absence of plant cell nuclei after staining samples for DNA (Hoechst, 5 min, 1:1000). The plant tissues fluoresce post-Hoescht staining, and the morphology of porous parenchyma was evaluated by quantifying pore morphology (diameter, roundness) using fluorescent microscope images and ImageJ (National Institute of Health, USA) software. Similarly, the morphology of fibrous vascular bundles was determined by staining celery tissue samples with Hoescht, followed by imaging and image analysis of fiber spacing and alignment. To assess the mechanical properties of the plant tissues, scaffolds pre and post decellularization were placed in 1 mL of PBS at 37 °C overnight. Bulk compressive moduli were then determined using a Shimadzu EZ-SX Mechanical Tester fitted with a compression clamp running at a constant strain rate of 10%/min in air at room temperature. The modulus was calculated from the slope of the stress–strain curve between 10 and 20% strain ($n \geq 3$). To obtain indentation moduli, porous and fibrous samples (both pre- and post-decellularization) were glued to a glass slide and hydrated for at least 30 min in PBS prior to testing. An Optics 11 Chiaro Nanoindentation system was used to apply a 500 nm indentation (43.5 μm radius spherical indenter, 5 μm/s). Load-indentation curves were fit with a Hertzian model, and only fits with an $R^2 > 0.90$ were included in analyzes.

Hydrogel Polymerization

Methacrylated gelatin (GelMe) was dissolved in PBS at 2 wt% with 0.05 wt% 2-hydroxy-4'-(2-hydroxyethoxy)-2-methylpropiophenone (I2959). The prepolymer solution (80 μL) was pipetted into a silicone mold (8 mm diameter, 2 mm height) and irradiated with UV light (10 min, 10 mW/cm^2). Individual hydrogels were removed from the molds and placed in 1 mL of PBS overnight at 37 °C. Compressive moduli were then determined using a Shimadzu EZ-SX Mechanical Tester fitted with a compression clamp running at a constant strain rate of 10%/min in air at room temperature. The modulus was calculated from the slope of the stress–strain curve between 10 and 20% strain ($n \geq 3$).

MSC Culture and Seeding

Human MSCs (Lonza) were cultured in MSC growth medium (formulation in Table S1). Low passage MSCs (P3 to P4) were thawed and plated on tissue culture plastic and cultured in growth medium at 37 °C in a humidity-controlled incubation chamber (5% CO_2) until reaching 80% confluency. Upon reaching 80% confluency, MSCs were detached with trypsin–EDTA (0.25%, Gibco) and either passaged or seeded onto decellularized plant tissues. For differentiation studies, MSCs were cultured in osteogenic (OS) or myogenic (MYO) medium using formulations listed in Table S1. Media changes were performed every other day unless cells were fixed on the day of a media change. MSCs were seeded on celery tissues at a concentration of 10,000 cells/cm^2 and cultured for 3 days for morphology and mechanosensing studies. For differentiation studies, MSCs acclimated for 12 h in MSC growth medium before changing to appropriate inductive media.

MSC Adhesion and Proliferation

To evaluate adhesion, porous and fibrous celery tissues were treated with Col (+) or without Col (−) rat-tail collagen (Corning) by soaking in collagen solution (3.08 mg/ml) for 8 h. MSCs were then cultured (10,000 cells/cm^2) for 3 days followed by fixation with 10% formalin (10 min), permeabilized with 0.1% Triton X-100 (2 min), and blocked with 3% bovine serum albumin (BSA, 30 min). Samples were then stained for actin (Alexa Fluor 568 phalloidin, 20 min, 1:100) and DNA (Hoechst, 5 min, 1:1000) followed by imaging. Cell adhesion was determined by counting stained nuclei using ImageJ software. To evaluate cell proliferation, samples were incubated in 500 μL alamarBlue working solution (MSC Growth Medium with 10% alamarBlue reagent, ThermoFisher) at 37 °C after 1, 3, 5, and 7 days (D1, D3, D5, D7) in culture. After 4 h, 50 μL aliquots of the working solution were transferred into wells of a 96-well plate, and the fluorescence was measured at an excitation/emission maxima of 560/590 nm with a plate reader.

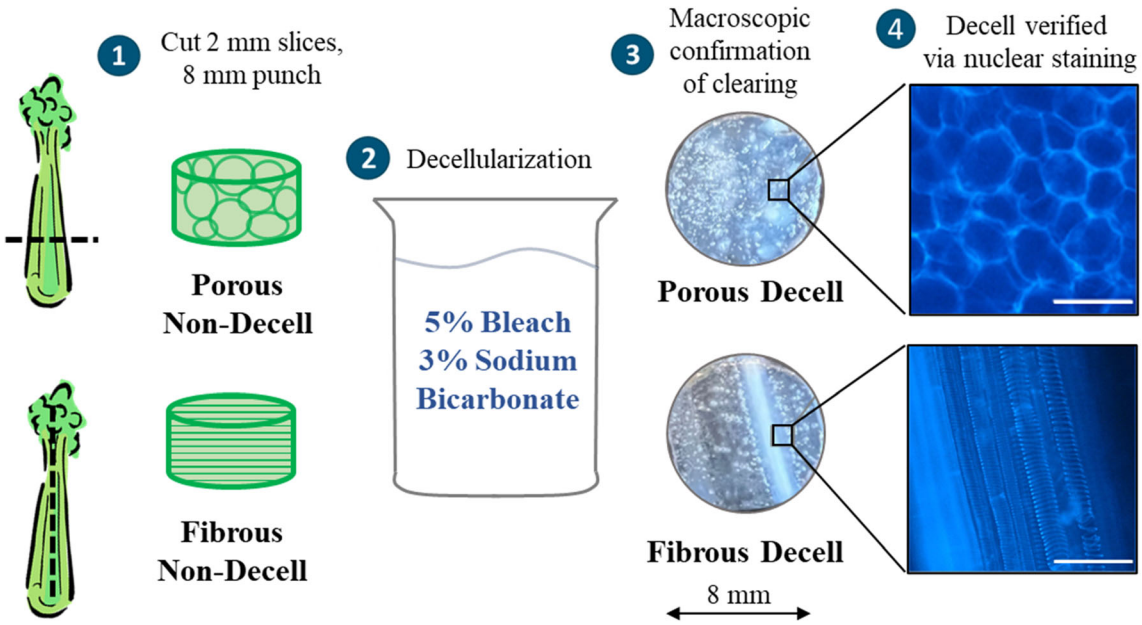

FIGURE 1. Scheme for preparing decellularized plant scaffolds. Celery stalks were cut cross-sectionally or longitudinally (2 mm thickness) and biopsy punched (8 mm diameter) to create non-decellularized (non-Decell) porous or fibrous tissues. Non-Decell samples were then decellularized resulting in porous and fibrous Decell tissue samples. Gross and microscopy images confirm that the macro and microarchitecture is conserved post-decellularization. Scale bars: 200 μm.

Immunostaining and Image Analysis

To evaluate MSC morphology and mechanosensing, MSCs were cultured on decellularized porous or fibrous plant tissues for 3 days and stained with actin, YAP (Santa Cruz Biotechnologies, 1:200, Alexa Fluor 488 secondary, 1:200), and Hoescht. Fluorescently labeled samples were imaged using a Nikon A1 confocal microscope. Cell shape descriptors (area, roundness, aspect ratio), actin alignment/anisotropy, and nuclear YAP localization were acquired from confocal images using ImageJ software. Nuclear YAP localization was determined by measuring the integrated density of YAP of five regions of interest (ROI) on the cytoplasm and nucleus of each cell, respectively. The ratio between the integrated density of the nuclear and cytoplasmic ROIs were defined as the nuclear YAP value.

To evaluate MSC differentiation, after 7 days in culture, samples were sequentially stained for MyoD (Santa Cruz Biotechnologies, 1:200, Alexa Fluor 488 secondary, 1:200) and alkaline phosphatase using Fast Blue (1.45 M Fast Blue RR Salt, 4% Naphthol AS-MX Phosphate, Sigma Aldrich, 1 h). Fast blue fluoresces upon deep red (640 nm) excitation, and acquisition of all immunofluorescence images was performed with a Nikon A1 confocal microscope. For analysis, maximum intensity z-projection images of the nucleus (blue), cell body (red), MyoD (green), and ALP (magenta) channels were obtained and converted to 8-bit images. To evaluate myogenic differentiation, the mean fluorescence intensity (MFI) of MyoD in the nucleus was quantified using ImageJ software.

To evaluate osteogenic differentiation, an ROI mask was created to measure the fluorescence of ALP in the cytoplasm while excluding the nucleus. The mask is a ring with an outer diameter determined by a quadruple dilation of the nucleus and inner diameter of the original nucleus. This mask was overlaid onto the ALP channel to generate rings of ALP fluorescence. The 3D Objects Counter tool on ImageJ was then used to calculate the area of the rings, and the Measurement tool was used to quantify the integrated density of the ALP rings. The corresponding MFI of every cell was calculated by taking the ratio between the integrated density and the area of the ring.

To determine the minimal MFI for an MSC to be classified as ALP or MyoD positive, MFI frequency distribution curves were used.[33] MSCs were cultured on flat GelMe hydrogels in Growth, OS, or MYO medium for 7 days followed by staining and imaging to acquire and plot MFI frequency distribution curves. The MFI values which were one standard deviation from the mean MFI (mean minus SD) of the OS or MYO cell curves were selected as thresholds for classifying an ALP or MyoD positive cell. Based on the minimal MFI (MFI $>$ 38 for positive MyoD; MFI $>$ 19 for positive ALP), the percentage of cells positive for MyoD and ALP was determined.

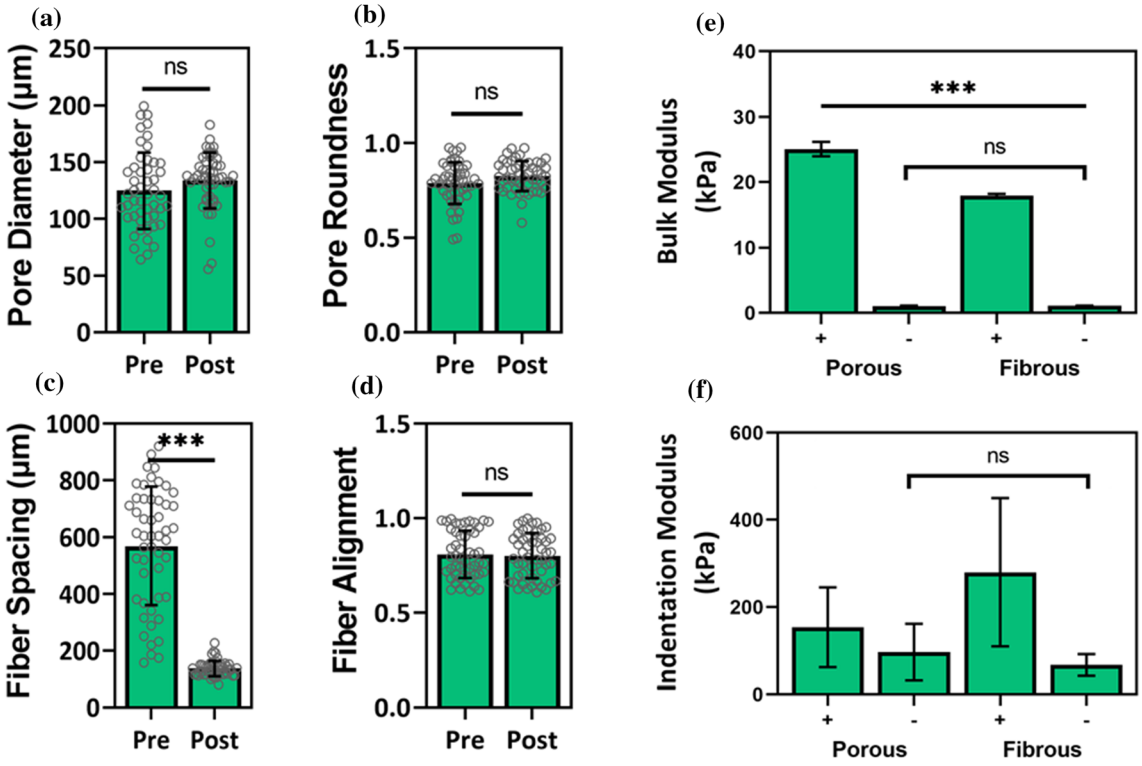

FIGURE 2. Plant scaffold characterization. Bar graphs of (a) pore diameter and (b) pore roundness pre and post decellularization. Bar graphs of (c) fibrous intrabundular spacing and (d) fiber alignment pre and post decellularization. (e) Indentation moduli of porous and fibrous celery tissues. (f) Bulk moduli of porous and fibrous celery tissues. Bar graphs shown as mean ± SD ($n \geq 3$ samples per condition). Significant and non-significant (ns) differences determined with ANOVA followed by Tukey's *post hoc* test where ***$p < 0.001$.

Statistical Analysis

Statistical analyses were performed using GraphPad Prism 9.3.1 software. All experiments were carried out in triplicates and single cell analysis was done with at least 50 cells per group. All graphs represent mean ± standard deviation (SD). For comparisons of three or more groups, normally distributed populations were analyzed *via* analysis of variance (ANOVA) with a Tukey's *post hoc* test to correct for multiple comparisons. Differences among groups are stated as $p < 0.05$ (*), $p < 0.01$ (**), or $p < 0.001$ (***). Differences between groups that are not statistically significant are denoted as (ns). Box plots show 25/50/75th percentiles, whiskers show minimum/maximum.

RESULTS AND DISCUSSION

Plant Tissue Microtopography is Conserved Post-Decellularization

A gentle detergent-free decellularization technique was applied to celery plant tissue samples to remove genetic and cellular material while maintaining native microtopographical features (Fig. 1). Cell nuclei were not visible post decellularization, indicating complete decellularization. This decellularization protocol was adapted from the work of Adamski and colleagues who compared this detergent-free decellularization to a detergent-based protocol.[1] Their experiments demonstrated that both protocols sufficiently remove cellular material while retaining delicate physical properties of the plant tissues. Due to the time-intensive nature of the detergent-based protocol, we utilized the detergent-free methods in these experiments.

The diameter of pores in the porous tissues remained the same pre and post decellularization, with values of 124 ± 33 μm and 133 ± 24 μm, respectively (Fig. 2a). Similarly, pore roundness remained the same pre and post decellularization, with values of 0.79 ± 0.11 and 0.82 ± 0.08, respectively (Fig. 2b). In fibrous tissues the intrabundular spacing or the width of every fiber decreased after decellularization from 569 to 136 μm (Fig. 2c). Pre decellularization, the intrabundular spacing or the width of every fiber was highly variable, with a standard deviation of 208 μm. Although the decellularization process resulted in an over two-fold decrease in intrabundular spacing, the fiber spacing became very reproducible and consistent across every sample, as seen by a much lower standard deviation. In addition to more consistent fiber

spacing, alignment (0 to 1, where 1 is perfectly aligned) was also high and preserved pre (0.81 ± 0.12) and post (0.81 ± 0.11) decellularization (Fig. 2d).

While microtopographical features were conserved post-decellularization, the mechanical properties of the porous and fibrous tissues decreased post decellularization. The bulk moduli of the porous tissues pre and post decellularization were 25.06 ± 1.10 kPa and 1.06 ± 0.07 kPa, respectively (Fig. 2e). Similarly, bulk moduli values of fibrous tissue pre and post decellularization were 17.90 ± 0.29 kPa and 1.09 ± 0.05 kPa, respectively. A bulk-stiffness matched GelMe hydrogel which lacks any significant microtopography was also synthesized as a control group for the MSC studies (Figure S1).

Due to potential differences in local mechanics arising from microtopographical features, a nanoindenter was used to determine mechanical properties at the microscale (Fig. 2f). The indentation moduli of porous and fibrous scaffolds pre-decellularization was significantly higher than the bulk moduli, suggesting that surface mechanical properties are enhanced by the microtopography, and this is not captured using bulk mechanical testing. Indentation moduli for fibrous scaffolds (283 ± 173 kPa) was also higher than porous scaffolds (154 ± 92 kPa) pre-decellularization, and this is likely due to increased material density from the highly aligned tissue and cellular material. Interestingly, the indentation moduli of decellularized porous (97 ± 65 kPa) and fibrous (67 ± 25 kPa) plant scaffolds were significantly higher than the bulk moduli of decellularized tissues (~ 1 kPa).

MSC respond to substrate stiffness,[11] and thus the large difference between bulk and indentation moduli is a critical nuance. These results highlight the importance of not only the macro-mechanical properties of biomaterials, but also mechanical properties present at the more relevant micro- and nano- scales. Taken together, these data indicate that it is possible to decellularize plant-derived scaffold materials to ensure biocompatibility, while protecting inherent physical properties that are difficult and costly to reproduce in synthetic scaffold materials.

MSCs Adhere and Proliferate on Decellularized Plant Tissues

Adherent cells must be able to attach to biomaterials for cell-material communication to occur. Since the decellularization process could reduce the availability and activity of adhesive domains, porous and fibrous celery tissues were coated with collagen to determine whether this would enhance MSC adhesion. To confirm improved adhesion, MSCs were cultured atop non-collagen-coated Col (−) or collagen-coated Col (+) celery tissues. Cell attachment after 3 days in culture was evaluated by counting nuclei on stained samples using ImageJ software. Porous and fibrous Col (+) tissues were observed to have higher cell attachment than Col (−) tissues (Fig. 3a). The differ-

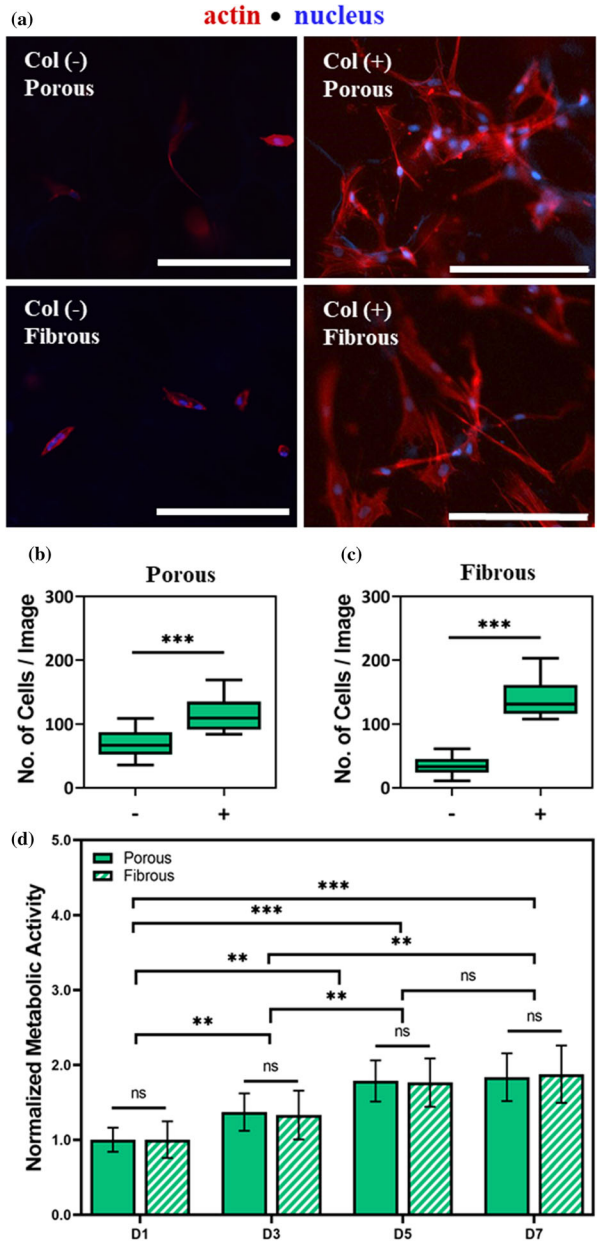

FIGURE 3. MSCs adhere and proliferate on decellularized porous and fibrous celery tissues. (a) Representative F-actin (red) and nuclear (blue) staining of MSCs seeded atop non-collagen coated Col (−) and collagen coated Col (+) celery tissues. Quantification of number of MSCs per image of Col (+) (b) porous and (c) fibrous celery tissues. (d) Normalized metabolic activity of MSCs on porous and fibrous celery tissues. Error bars shown as SD ($n \geq 3$ samples per condition). Significant and non-significant (ns) differences determined with ANOVA followed by Tukey's *post hoc* test where *$p < 0.05$, **$p < 0.01$, ***$p < 0.001$. Scale bars: 200 μm.

ence between Col (−) and Col (+) on porous tissues was 69 ± 21 and 117 ± 30 adherent cells per image, respectively (Fig. 3b). When comparing Col (−) and Col (+) on fibrous tissues, the difference was much larger, with average cell counts reported as Col (−) 34 ± 13 and Col (+) 141 ± 32 (Fig. 3c). On GelMe hydrogels of comparative bulk stiffness, collagen coating had no effect on cell attachment, with Col (−) and Col (+) GelMe values of 60 ± 11 and 57 ± 18, respectively (Figure S2). Since the collagen coating improved MSC adhesion, collagen-coated scaffolds were used for all cellular experiments.

To evaluate cell proliferation on porous and fibrous celery tissues, MSCs were seeded atop Col (+) celery tissues and cellular metabolic activity was determined after 1, 3, 5, and 7 days (D1, D3, D5, D7) in culture. An increase in metabolic activity was observed at every time point for both porous and fibrous tissue groups with approximately two times the initial metabolic activity on Day 7 (Fig. 2d). Meanwhile, no differences were observed between the fibrous and the porous microtopographies at any given time point. On GelMe hydrogels of comparable bulk mechanics, cellular metabolic activity on Day 1 was approximately half that of the celery plant tissue and increased to less than 1.5 times the initial metabolic activity by Day 7 (Figure S3). These results indicate that MSCs cultured on porous and fibrous celery tissues adhere and proliferate even more readily than on the commonly used GelMe hydrogels, which lack microtopography.

These results indicate that though cells adhere naturally to plant-derived scaffolds, adhesion to these materials is significantly improved with the addition of biofunctional molecules like collagen. Interestingly, porous microtopographies exhibited higher levels of Col (−) adhesion than on non-collagen treated fibrous scaffolds. We hypothesize that the higher baseline MSC adhesion on porous tissues may be due to a higher surface area available for adhesion from the porous microtopography.[31] Further, these results indicate that the presence of microtopography could also have a positive relationship with the proliferative capacity of stem cells, an important consideration when designing cell-laden biomaterials. Ultimately, the addition of other biofunctional molecules to plant-derived scaffolds could be an avenue for improving the versatility and tunability of these materials.

MSC Morphology is Influenced by Plant Tissue Microtopography

To evaluate the morphological behavior of MSCs on decellularized plant tissues, MSC were cultured atop porous and fibrous celery tissues for 3 days and microtopography-driven changes in morphological parameters (area, roundness, aspect ratio) were evaluated. Representative images of MSCs on porous (Fig. 4a) and fibrous (Fig. 4b) celery tissues show distinct differences in morphology. MSCs on porous tissues were significantly smaller (1232 ± 407 μm^2) than MSCs on fibrous tissues (1954 ± 601 μm^2) (Fig. 4c). MSCs were also significantly rounder on porous tissues (Fig. 4d) and had a larger aspect ratio on fibrous tissues (Fig. 4e). MSC morphology atop fibrous celery tissues were consistent with the morphology of MSCs atop GelMe hydrogels of comparable bulk stiffness. MSCs on GelMe hydrogels have an area of 1950 ± 79 μm^2, roundness of 0.32 ± 0.17, and aspect ratio of 2.67 ± 1.80 (Figure S4).

These results show that the differences in topographical features between porous and fibrous celery tissues result in distinct morphologies of cultured MSCs, a critical finding given the established relationship between MSC morphology and downstream lineage commitment.[20,25] This finding supports the idea that the inherent physical properties of plant-derived tissue engineering scaffolds can independently influence the behavior of stem cells.

MSC Mechanosensing on Fibrous Vascular Bundles is Higher than in Porous Parenchyma

To further evaluate the extent to which 2D mechanical cues from distinct microtopography of celery tissues influence cellular mechanosensing, the presence and location of intracellular mechanosensitive proteins were assessed. The protein YAP is a key transducer of mechanical signals, and MSCs express and increase in nuclear YAP localization with increasing mechanical stimulation.[10]

After 3 days in culture atop celery tissues, nuclear YAP on the fibrous group was higher than the porous group (Fig. 5a), with values of 2.00 ± 0.41 on porous and 2.82 ± 0.89 on fibrous celery tissues (Fig. 5b). This is not surprising, since the fibrous microarchitecture also induced an increase in MSC area and aspect ratio, suggesting a more contractile, mechanoactive state (Figs. 4c, 4e). Nuclear YAP values on soft GelMe hydrogels were lower than porous or fibrous (Figure S5a), further demonstrating that plant microarchitecture can enhance nuclear YAP, and thus cellular mechanosensing. Actin anisotropy (actin fiber alignment) is a measure of the organization of actin stress fibers, and there was also a significant increase in actin anisotropy (0.18 ± 0.05 vs. 0.33 ± 0.05) between MSCs in porous and fibrous celery tissues (Figs. 5c, 5d). Actin alignment on soft GelMe hydrogels was lower than on celery tissues with microarchitecture (Figure S5b).

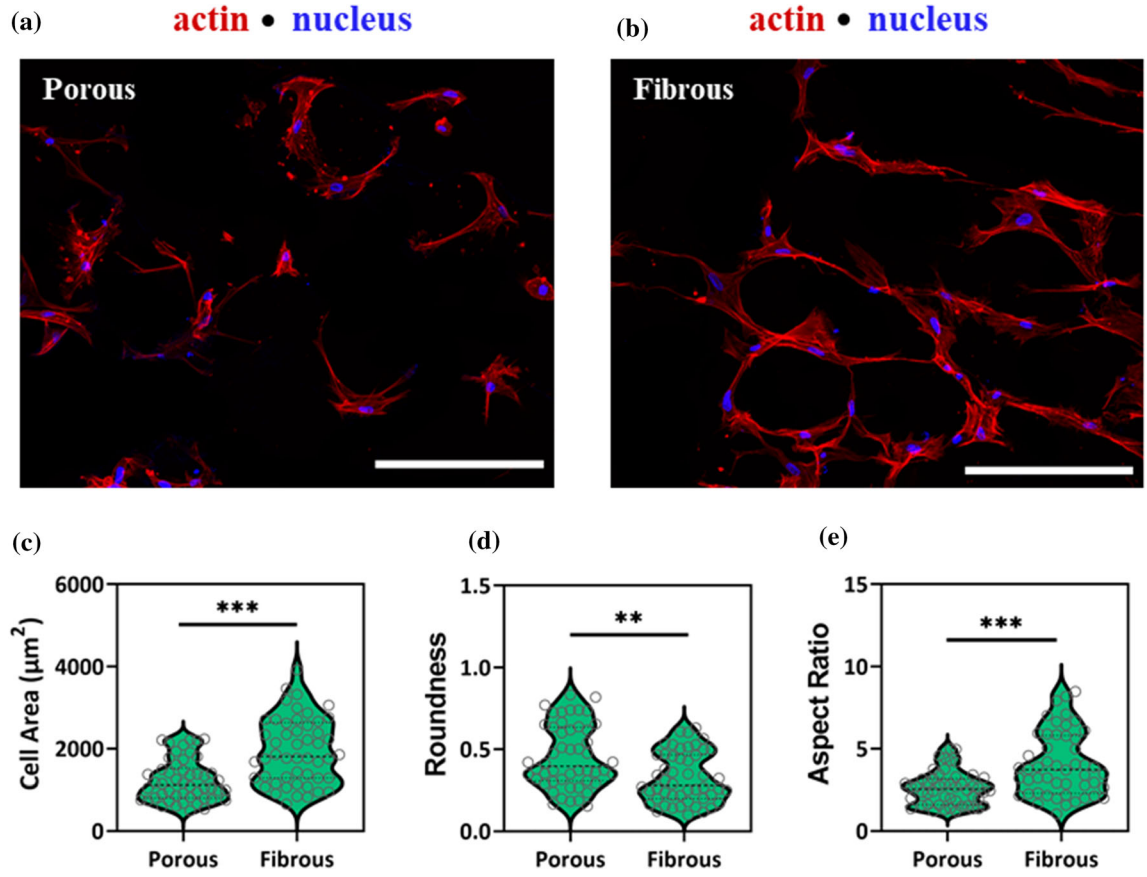

FIGURE 4. MSC morphology is influenced by plant tissue topography. Representative F-actin *(red)* and nuclear *(blue)* staining of MSCs seeded atop (a) porous and (b) fibrous celery tissues. Quantification of cell (c) area, (d) roundness, and (e) aspect ratio. Sample size is $n \geq 50$ cells per condition with significant differences determined with ANOVA followed by Tukey's *post hoc* test where $^{**}p < 0.01$, $^{***}p < 0.001$. Scale bar: 200 μm.

Taken together, these results show that topographies that cause an increase in cell area and aspect ratio also enhance MSC mechanosensing. Cellular mechanical activity has been shown to have important implications for stem cell differentiation and developing biomaterials with properties that encourage directed differentiation is of considerable scientific and clinical interest. These results indicate that physical properties beyond stiffness alone can be leveraged to drive stem cell mechanosensing and ultimately differentiation.

MSC Lineage Commitment Based on Plant Tissue Microtopography

Cellular mechanosensing plays a large role in directing MSC differentiation.[9,19,34] On aligned microgrooves, the expression of myogenic biomarkers increases with MSC alignment.[34] In contrast, porosity of ceramic materials enhance MSC differentiation into osteoblasts *in vitro* and *in vivo*.[19] To assess the effects of the porous and fibrous topographical features of celery tissues on MSC lineage commitment, MSCs were seeded atop porous or fibrous celery tissues and cultured in growth, OS, or MYO medium. After 7 days in culture, samples were fixed and sequentially stained for bone and muscle biomarkers ALP and MyoD, respectively, then counterstained with phalloidin (cell body) and Hoescht (nuclei). To minimize bias in identifying MSCs as ALP or MyoD positive, MSCs were also cultured in Growth, OS, or MYO medium on flat GelMe hydrogels for 1 week and the mean fluorescence intensity (MFI) was plotted as Growth vs. OS (Fig. 6a) and Growth vs. MYO (Fig. 6b) histograms. The cutoff MFI for ALP was then determined by subtracting the mean OS MFI value by one standard deviation, shown as a vertical dashed line in Fig. 6a. A similar process was employed to determine the cutoff MFI for MyoD, and a threshold MFI of 19 and 38 were found for ALP and MyoD, respectively.

In osteogenic medium, MSCs on porous celery tissues had a stronger ALP expression in comparison to the fibrous group as seen by higher ALP fluorescence intensity (magenta) (Fig. 6c). Percentage of ALP-ex-

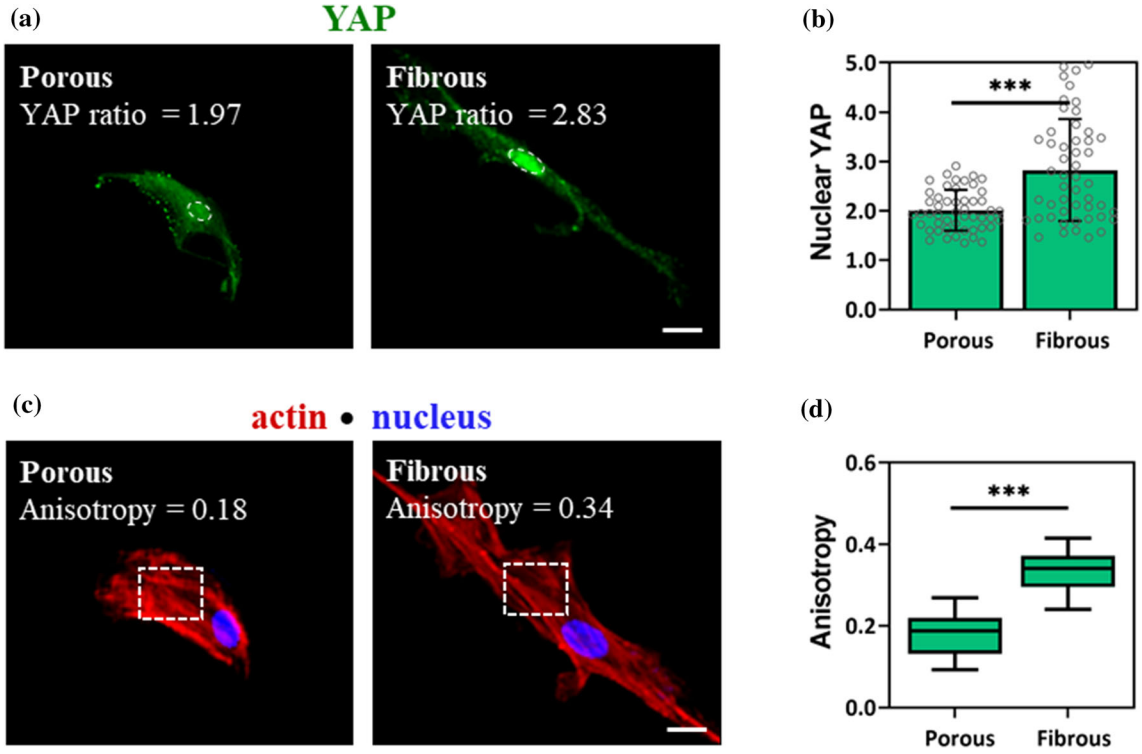

FIGURE 5. MSC mechanosensing on fibrous vascular bundles is higher than in porous parenchyma. (a) Representative YAP *(green)* staining with outlined nuclei *(dashed oval)* of MSCs on porous or fibrous celery tissues. (b) Quantification of nuclear YAP ratio. (c) Representative F-actin *(red)* and nuclear *(blue)* staining of MSCs with region of interest for actin anisotropy measurement *(dashed rectangle)*. (d) Quantification of actin anisotropy. Error bars are shown as SD ($n \geq 50$ cells per condition) with significant differences determined with ANOVA followed by Tukey's *post hoc* test where ***$p < 0.001$. Scale bar: 20 μm.

pressing cells using an MFI cutoff of 19 (MSCs are classified as ALP-positive if their MFI is greater than 19) was 98 ± 2% on porous celery tissues and significantly lower (70 ± 5%) on fibrous plant tissues (Fig. 6d). Remarkably, nearly every single MSC on porous celery tissues analyzed expressed ALP. Conversely, MSCs on fibrous tissues had a higher intensity of MyoD fluorescence (green) compared to MSCs on porous tissues (Fig. 6e), with positive cell response for MyoD of 24 ± 6 and 82 ± 5% on porous and fibrous tissues, respectively (Fig. 6f). Notably, there is a greater than threefold increase in MyoD expressing cells on the fibrous celery tissue when compared to the porous tissues. Further, certain groups exhibited heightened levels of ALP or MyoD expression on plant scaffolds in the absence of inductive media (Figure S6). On porous celery tissues cultured in Growth medium, the positive cell response was determined to be 49 ± 2 and 6 ± 3% for ALP and MyoD, respectively (Figure S6c). Similarly on fibrous tissues, the positive cell response was determined to be 39 ± 6 and 40 ± 7% for ALP and MyoD, respectively (Figure S6c).

Taken together, these results indicate that the microtopography of plant scaffolds can be leveraged to enhance the differentiation potential of MSCs. The effects of soluble growth factors on MSC differentiation are particularly improved when the underlying microtopography of the plant tissue reflects that of the desired native tissue (porous parenchyma that mimic cancellous bone and fibrous bundles that to mimic skeletal muscle). When cultured in OS medium, nearly all MSCs cultured on porous parenchyma expressed the bone biomarker, ALP. Further, MyoD was expressed at significantly higher rates in MSCs on fibrous (muscle-mimicking) than on porous celery tissues. Surprisingly, the bulk and indentation moduli differences between the porous and fibrous materials were shown to be insignificant, decoupling substrate stiffness from the improved differentiation capacities from microtopographical features alone. Where these features are often difficult and costly to reproduce in synthetic materials, nature has provided us with a diverse array of plant scaffold materials with properties reflective of native human tissues to choose from.

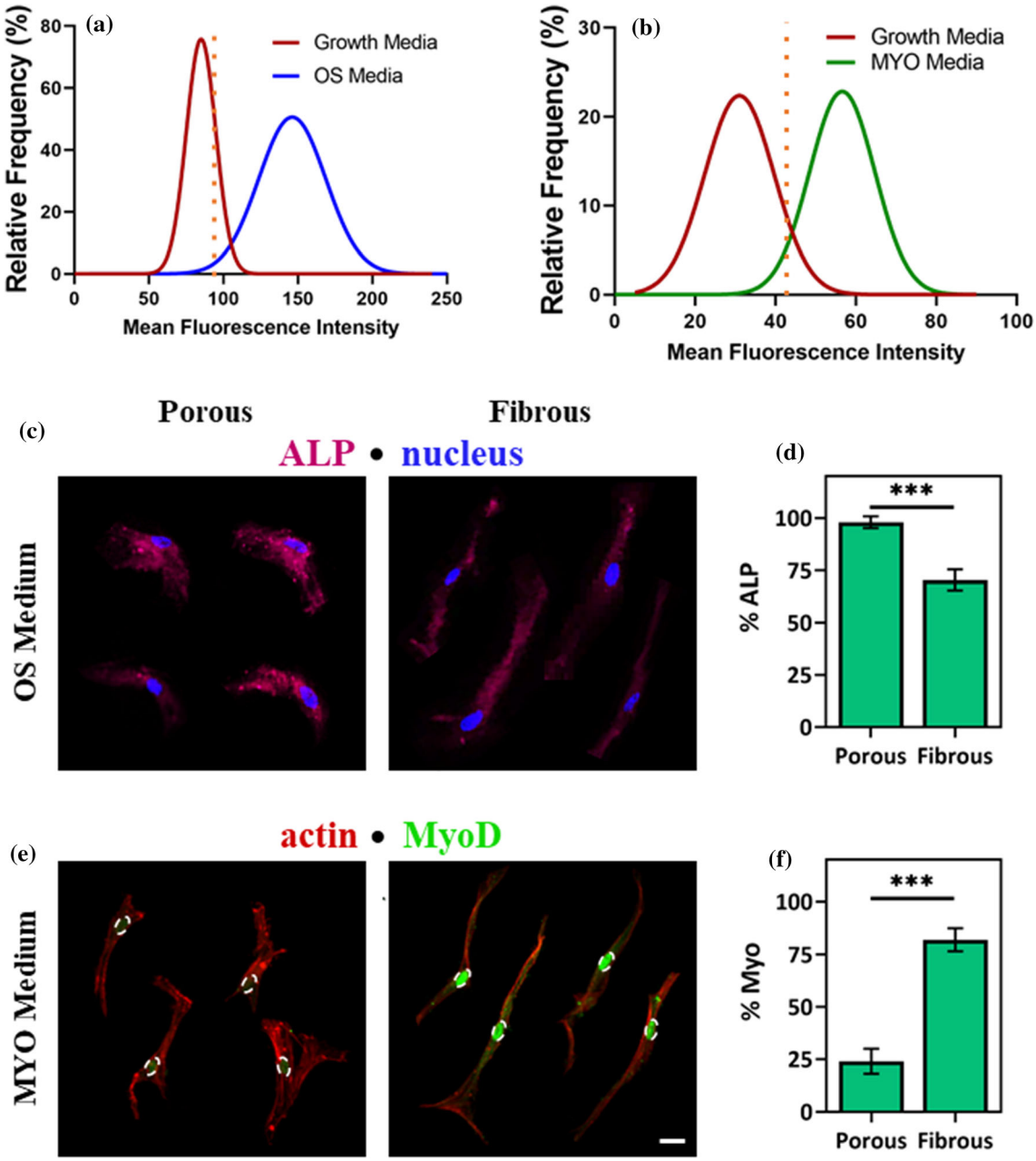

FIGURE 6. MSC lineage commitment based on plant tissue microtopography. Frequency distribution of mean fluorescence intensity (MFI) of MSCs seeded atop flat GelMe hydrogels for (a) ALP and (b) MyoD analysis. (c) Representative ALP (magenta) and nuclear (blue) staining of MSCs cultured on porous or fibrous celery tissues in OS medium. (d) Quantification of ALP positive MSCs on porous and fibrous celery tissues. (e) Representative MyoD (green) and F-actin (red) staining of MSCs cultured on porous or fibrous celery tissues in MYO medium. (f) Quantification of MSCs positive for MyoD expression. Bar graphs are shown as mean ± SD ($n \geq 50$ cells per condition) with significant differences determined with ANOVA followed by Tukey's *post hoc* test where ***$p < 0.001$. Scale bar: 20 μm.

CONCLUSIONS

In this study, celery stalks were cut cross-sectionally or longitudinally to expose distinct microtopographies. These microtopographies were shown to influence MSC morphology, mechanosensing, and downstream differentiation in inductive media. Through these experiments, we have sought to demonstrate that given their biocompatibility, low-cost, and structural complexity, plant-derived biomaterials are uniquely suited for use as tissue engineering scaffolds.

Future work in this area should include an exploration of other microtopographies and structural elements inherent in nature, as well as a more in-depth analysis of the host immune reaction to and degradation kinetics of these biomaterials *in vivo*. Further functionalizing plant-derived tissue scaffolds with biofunctional molecules also offers a promising avenue for exploration. Ultimately, the potential future applications for plant-derived biomaterials are only limited by the diversity of the plant kingdom itself.

SUPPLEMENTARY INFORMATION

The online version of this article contains supplementary material available https://doi.org/10.1007/s12195-022-00737-9.

ACKNOWLEDGMENTS

This work was supported by the National Science Foundation (DMR-2037055), Department of Veteran Affairs (IK2 RX003928), and a Sigma Xi Grant in Aid of Research (GIAR) Award (G03152021115818784).

CONFLICT OF INTEREST

K.D., M.S.B., K.A.G., A.M., J.M.P., and S.L.V. declare that they have no conflict of interest.

ETHICAL APPROVAL

No animal or human studies were carried out by the authors for this article.

REFERENCES

[1]Adamski, M., G. Fontana, J. R. Gershlak, G. R. Gaudette, H. D. Le, and W. L. Murphy. Two methods for decellularization of plant tissues for tissue engineering applications. *J. Vis. Exp.* 135:e57586, 2018.

[2]Bilirgen, A. C., M. Toker, S. Odabas, A. K. Yetisen, B. Garipcan, and S. Tasoglu. Plant-based scaffolds in tissue engineering. *ACS Biomater. Sci. Eng.* 7(3):926–938, 2021.

[3]Carlsbecker, A., Y. Helariutta, G. Coupland, and S. P. Monguio. Phloem and xylem specification: pieces of the puzzle emerge This review comes from a themed issue on Cell signalling and gene regulation Edited by. *Curr. Opin. Plant Biol.* 8:512–517, 2005.

[4]Chen, C., Y. Zhu, R. Wang, Y. Han, and H. Zhou. Effect of controlled microtopography on osteogenic differentiation of mesenchymal stem cells. *J. Healthc. Eng.* 1–10, 2022.

[5]Cheng, Y. W., D. J. Shiwarski, R. L. Ball, K. A. Whitehead, and A. W. Feinberg. Engineering aligned skeletal muscle tissue using decellularized plant-derived scaffolds. *ACS Biomater. Sci. Eng.* 6:3046–3054, 2020.

[6]Contessi Negrini, N., N. Toffoletto, S. Farè, and L. Altomare. Plant tissues as 3D natural scaffolds for adipose, bone and tendon tissue regeneration. *Front. Bioeng. Biotechnol.* 8:723, 2020.

[7]Crang, R., S. Lyons-Sobaski, and R. Wise. Parenchyma, Collenchyma, and Sclerenchyma. *Plant Anatomy* 181–213, 2018.

[8]Cun, X., and L. Hosta-Rigau. Topography: a biophysical approach to direct the fate of mesenchymal stem cells in tissue engineering applications. *Nanomaterials.* 10:2070, 2020.

[9]Dalby, M. J., et al. The control of human mesenchymal cell differentiation using nanoscale symmetry and disorder. *Nat. Mater.* 6:997–1003, 2007.

[10]Dupont, S., et al. Role of YAP/TAZ in mechanotransduction. *Nature.* 474:179–83, 2011.

[11]Engler, A. J., S. Sen, H. L. Sweeney, and D. E. Discher. Matrix elasticity directs stem cell lineage specification. *Cell.* 126:677–689, 2006.

[12]Gershlak, J. R., et al. Crossing kingdoms: using decellularized plants as perfusable tissue engineering scaffolds. *Biomaterials.* 125:13–22, 2017.

[13]Green, D. W., G. S. Watson, J. A. Watson, D. J. Lee, J. M. Lee, and H. S. Jung. Diversification and enrichment of clinical biomaterials inspired by Darwinian evolution. *Acta Biomater.* 15(42):33–45, 2016.

[14]Guilak, F., D. M. Cohen, B. T. Estes, J. M. Gimble, W. Liedtke, and C. S. Chen. Control of stem cell fate by physical interactions with the extracellular matrix. *Cell Stem Cell.* 5:17–26, 2009.

[15]Halder, G., S. Dupont, and S. Piccolo. Transduction of mechanical and cytoskeletal cues by YAP and TAZ. *Nat. Rev. Mol. Cell Biol.* 13:591–600, 2012.

[16]Heng, B. C., et al. Role of YAP/TAZ in cell lineage fate determination and related signaling pathways. *Front. Cell Dev. Biol.* 8:735, 2020.

[17]Insuasti-Cruz, E., et al. Natural biomaterials from biodiversity for healthcare applications. *Adv. Healthc. Mater.* 11(1):2101389, 2022.

[18]Iravani, S., and R. S. Varma. Plants and plant-based polymers as scaffolds for tissue engineering. *Green Chem.* 21:4839–4867, 2019.

[19]Kasten, P., I. Beyen, P. Niemeyer, R. Luginbühl, M. Bohner, and W. Richter. Porosity and pore size of β-tricalcium phosphate scaffold can influence protein production and osteogenic differentiation of human mesenchymal stem cells: an in vitro and in vivo study. *Acta Biomater.* 4:1904–1915, 2008.

[20]Kilian, K. A., B. Bugarija, B. T. Lahn, and M. Mrksich. Geometric cues for directing the differentiation of mesenchymal stem cells. *Proc. Natl. Acad. Sci. U.S.A.* 107:4872–4877, 2010.

[21]Kimura, K., et al. Regulation of myosin phosphatase by Rho and Rho-associated kinase (Rho- kinase). *Science (80-).* 273:245–248, 1996.

[22]Lewis, Y. S. Spices and Herbs for the Food Industry. Orpington: Food Trade Press, 1984.

[23]MacIntosh, B.R., P.F. Gardiner, and A.J. McComas. Skeletal Muscle: Form and Function. edited by H. Kinetics. Human Kinetics, 2006.

[24]McBeath, R., D. M. Pirone, C. M. Nelson, K. Bhadriraju, and C. S. Chen. Cell shape, cytoskeletal tension, and RhoA regulate stem cell lineage commitment several studies have

noted that changes in cell shape themselves can alter the differentiation of precommitted mesenchymal lineages. *Dev. Cell.* 6(4):483–95, 2004.
[25]McBeath, R., D. M. Pirone, C. M. Nelson, K. Bhadriraju, and C. S. Chen. Cell shape, cytoskeletal tension, and RhoA regulate stem cell lineage commitment. *Dev. Cell.* 6:483–495, 2004.
[26]Milovanovic, P., et al. Porotic paradox: distribution of cortical bone pore sizes at nano- and micro-levels in healthy vs. fragile human bone. *J. Mater. Sci. Mater. Med.* 28:71, 2017.
[27]Modulevsky, D.J., C.M. Cuerrier, and A.E. Pelling. Biocompatibility of Subcutaneously Implanted Plant-Derived Cellulose Biomaterials. *PLoS One* 11, 2016.
[28]Modulevsky, D. J., C. Lefebvre, K. Haase, Z. Al-Rekabi, and A. E. Pelling. Apple derived cellulose scaffolds for 3D mammalian cell culture. *PLoS ONE.* 9:97835, 2014.
[29]Salehi, A., M. A. Mobarhan, J. Mohammadi, H. Shahsavarani, M. A. Shokrgozar, and A. Alipour. Efficient mineralization and osteogenic gene overexpression of mesenchymal stem cells on decellularized spinach leaf scaffold. *Gene.* 757:144852, 2020.
[30]Sowbhagya, H. B. Chemistry, technology, and nutraceutical functions of celery (*Apium graveolens* L.): an overview. *Crit. Rev. Food Sci. Nutr.* 54:389–398, 2014.
[31]Stevens, M. M., and J. H. George. Exploring and engineering the cell surface interface. *Science (80-).* 310:1135–1138, 2005.
[32]Thimm, J. C., D. J. Burritt, W. A. Ducker, and L. D. Melton. Celery (*Apium graveolens* L.) parenchyma cell walls examined by atomic force microscopy: effect of dehydration on cellulose microfibrils. *Planta.* 212:25–32, 2000.
[33]Vega, S. L., et al. High-content imaging-based screening of microenvironment-induced changes to stem cells. *J. Biomol. Screen.* 17:1151–1162, 2012.
[34]Wang, P. Y., W. T. Li, J. Yu, and W. B. Tsai. Modulation of osteogenic, adipogenic and myogenic differentiation of mesenchymal stem cells by submicron grooved topography. *J. Mater. Sci. Mater. Med.* 23:3015–3028, 2012.
[35]Use of Laboratory Animals in Biomedical and Behavioral Research. Use Lab. Anim. Biomed. Behav. Res. National Academies Press, 1988.